

CMOD5

Siebren de Haan and Ad Stoffelen

19 November 2001

Contents

1	Introduction	1
2	Geophysical model functions	3
3	Construction of CMOD5	4
3.1	Low and medium wind bias correction	4
3.2	High wind correction	5
4	CMOD5 performance	8
4.1	CMOD5 compared to other GMFs	9
4.2	Comparison with ECMWF 10 meter wind	12
4.3	High wind cases	18
5	Conclusions	22

1 Introduction

The European Remote Sensing (ERS-1 and -2) satellites were launched in 1991 and 1995. The ERS satellite circles the Earth at a height of 800 km and completes an orbit every 100 minutes crossing both poles in the process. In this so-called polar orbit, the Earth is gradually rotating beneath the spacecraft and so on each subsequent orbit a slightly different part of the ground is seen. Using this type of orbit the ERS-2 scatterometer can observe the surface of the entire globe almost completely in just three days. The only part which is not seen has a latitude higher than approximately 80° (Arctic) or lower than -80° (Antarctic).

Three antennas look in three different directions with radar look angles 45° , 90° and 135° (fore-, mid-, and aft-beam) relative to the flight direction, covering a

500 km wide swath parallel to the sub-satellite track. The ground swath is divided in regular grid nodes which have a 25 km size representing overlapping footprints of size 50 km. A scatterometer node is subsequently illuminated by each antenna resulting in a triplet of measured σ_0 . Across track the swath is divided in 19 cells with incidence angles, θ , ranging from 25° to 57° for the fore and aft beam and 18° to 46° for the mid beam. Over water σ_0 is related to wind speed, relative wind direction and incidence angle through an empirically derived model function. Using the three measurements obtained from three different directions surface wind speed and wind direction can be derived.

Satellite derived surface winds have proven to be very valuable for numerical weather prediction. From 1991 up to 2001 the ERS-1 and -2 scatterometer winds were operationally used at the European Centre for Middle Range Weather Forecasting (ECMWF). Scatterometer winds are obtained from backscatter measurements using a geophysical model function (GMF). The currently used GMF at ECMWF is the so-called CMOD4 GMF [Stoffelen (1997b)].

Recent unprecedented experimental work by [Donnelly (1999)] showed that these scatterometer winds underestimate high wind speeds. They presented normal radar cross sections (NRCS) for wind speeds as high as 45 ms^{-1} . They observed that the C-band NRCS sensibility decreases for wind speeds greater than 20 ms^{-1} . [Carswell (1999)] presented NRCS observations for even higher wind speeds up to 60 ms^{-1} . Both studies showed that CMOD4 over predicts the NRCS of the ocean surface for high wind speeds. Furthermore Carswell showed that the NRCS has a saturation behaviour at a certain wind speed, although distinct when different incidence angles are considered.

CMOD4 is known to have a bias at low and medium wind speeds. Triple collocation data with buoy winds, NCEP model winds and ERS scatterometer winds showed a first order bias in the wind speed of the order of 4 % and a higher order speed-dependent bias [Stoffelen (1998)].

In this text we describe a new GMF based on CMOD4 with a low and medium wind speed bias correction and a high wind speed behaviour as observed by Donnelly and Carswell. In the next second the GMFs are briefly explained. Section 3 shows the construction of a projection of the wind domain. In section 4 the constructed new GMF is compared to the observed backscatter observations of both Donnelly and Carswell. Section 4.2 contains a comparison of ECMWF derived 10 meter wind observations with scatterometer winds derived using the new GMF for a data set with a mean wind speed of around 14 ms^{-1} . The last section contains the conclusions.

2 Geophysical model functions

The currently widely used formulation of the ocean surface normalized radar cross section (NRCS) geophysical model function (GMF) is based on a truncated Fourier series in wind direction. The distinction between different GMFs is based on different functions to describe the wind speed and incidence angle dependence. The basic approximation is

$$\sigma_0 = B_0(1 + B_i \cos i\phi), \quad (1)$$

where ϕ is the wind-direction B_i depends on both the incidence angle θ and the wind speed v . The term B_0 is the mean NRCS backscatter. The first harmonic term, B_1 , represents the difference in backscatter between a wind up the beam versus down the beam. The second harmonic term, B_2 , represents the difference in backscatter of a wind blowing up or down compared to a wind blowing across the beam.

We first focus on the mean NRCS B_0 , because this term has the most pronounced wind speed dependence. The wind dependence (and incidence angle dependence) for CMOD4 of the mean NRCS B_0 is approximately given by (see for more details [Stoffelen (1997b)])

$$B_0^{\text{CMOD4}} \approx 10^{\alpha + \gamma f_1(V + \beta)}, \quad (2)$$

where α and γ depend on θ , β is a parabolic function in θ and the function f_1 is a piecewise function consisting of a constant part, a logarithmic part and a part with a square root dependence (see [Stoffelen (1997b)]).

[Donnelly (1999)] fitted the high wind mean NRCS, B_0 as

$$B_0^{\text{CMOD4HW}} = 10^{\beta + \gamma \log(V)}, \quad (3)$$

where β and γ have an incidence angle dependence. [Carswell (1999)] added an extra term to obtain observed saturation behaviour of the mean NRCS

$$B_0^{\text{HighWind}} = 10^{\beta + \gamma_1 \log(V) + \gamma_2 (\log(V))^2} \quad (4)$$

Both Donnelly and Carswell estimated the parameters carefully by using minimization algorithms applied on a series of airborne scatterometer measurements. Their estimations will be guide for an improvement of CMOD4.

Later we will see that the chosen method of improvement of CMOD4 will influence the behaviour of the first harmonic. The second harmonic is almost unaffected by the chosen improvements and therefor will not be discussed here. The first harmonic as defined for CMOD4 is

$$B_1^{\text{CMOD4}} = c_{10} + c_{11}V(c_{12} + c_{13})f_2((\theta - 40)/25), \quad (5)$$

where

$$f_2(x) = \tanh(2.5(x + 0.35)) - 0.61(x + 0.35) \quad (6)$$

The first harmonics of the CMOD4HW and HighWind have both a linear dependence on the wind speed, with different linear coefficients for different incidence angles θ , see [Donnelly (1999)] and [Carswell (1999)] for details.

3 Construction of CMOD5

The GMF CMOD4 is known to underestimated high wind speeds and contain a bias for medium and low wind speeds. To solve these problems a new GMF is constructed starting from CMOD4. A mapping of the wind speed is applied to reduce the bias for low and medium wind speeds and to establish a better high wind speed behaviour. The wind speed transformation will only be applied to the mean NRCS B_0 for high wind speeds. For low and medium winds the transformation is applied to all harmonics. The first harmonic B_1 of CMOD4 is scaled for high wind speeds.

The wind speed transformations is a mapping of the 'true' wind speed onto the CMOD4 wind speed. The wind speed transformation is split up into two parts: low and medium wind speed transformation and a high wind speed transformation, both discussed below.

3.1 Low and medium wind bias correction

The low wind bias correction is based on triple collocation of buoy data, NCEP model winds and ERS scatterometer winds. In such global wind data sets a first order bias of 4% is observed. The higher-order bias correction is shown in Fig. 1. The difference between the scatterometer wind and the buoy wind is plotted versus the buoy wind. Also shown in this figure is a fit based on a sine function with a wind speed dependent amplitude and phase. The fit is

$$\Delta v = \beta_0(v) \sin(\beta_1(v)), \quad (7)$$

where v is the 'true' wind speed. The functions β_i given by

$$\begin{aligned} \beta_0(v) = & 1.633484954 - .4122184703v \\ & +.477571668 \cdot 10^{-1}v^2 - .1626544 \cdot 10^{-2}v^3 \end{aligned} \quad (8)$$

$$\begin{aligned} \beta_1(v) = & .9245303434 - .1293527070v \\ & +.423168296 \cdot 10^{-1}v^2 - .1717568 \cdot 10^{-2}v^3 \end{aligned} \quad (9)$$

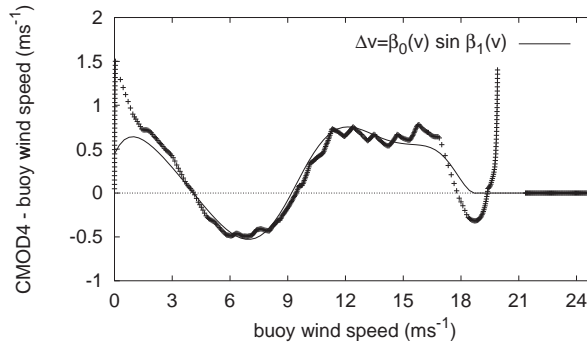


Figure 1: Higher-order calibration by cumulative distribution mapping of NOAA buoy anemometer and ERS scatterometer winds, see [Stoffelen (1998)].

The wind speed \bar{v} of CMOD4 corresponding to the true wind v becomes:

$$\bar{v} = \begin{cases} v/1.04 + \beta_0(v) \sin(\beta_1(v)) & v \leq 19 \text{ms}^{-1} \\ v/1.04 & v > 19 \text{ms}^{-1} \end{cases} \quad (10)$$

Following the method of simultaneous error modeling and calibration of triple collocated data described in [Stoffelen (1998)] the performance of the low and medium wind bias correction for both CMOD4 and CMOD5 is shown in Fig. 2. The bias in the wind speed obtained by using CMOD4 GMF in addition to the above described low wind bias correction with respect to the NOAA buoy wind is smaller than the corresponding bias from the uncorrected CMOD4 GMF, see Fig. 2 top panel. This is not surprising because the same data set was used to estimate the bias. More reassuring is the fact that the bias of the NCEP wind with respect to the scatterometer wind, shown in the bottom panel, is also reduced for wind speeds lower than approximately 15ms^{-1} . Scatterometer wind speeds higher than 15ms^{-1} are known to be incorrect; this problem is tackled in the next section where a high wind speed correction is developed.

3.2 High wind correction

Taking into account the corrections described above, the CMOD4 GMF overestimates high wind speed NRCS as shown by Donnelly and Carswell. To overcome this problem we perform a wind domain projection from the high wind speeds ('true' wind) onto lower wind speeds (CMOD4 wind). In this way the CMOD4 GMF can be altered such that it fits the measured high wind NRCS better.

The high wind speed transformation is the identity for wind speeds lower than 15ms^{-1} and has an asymptotic behaviour for high wind speeds. The general wind

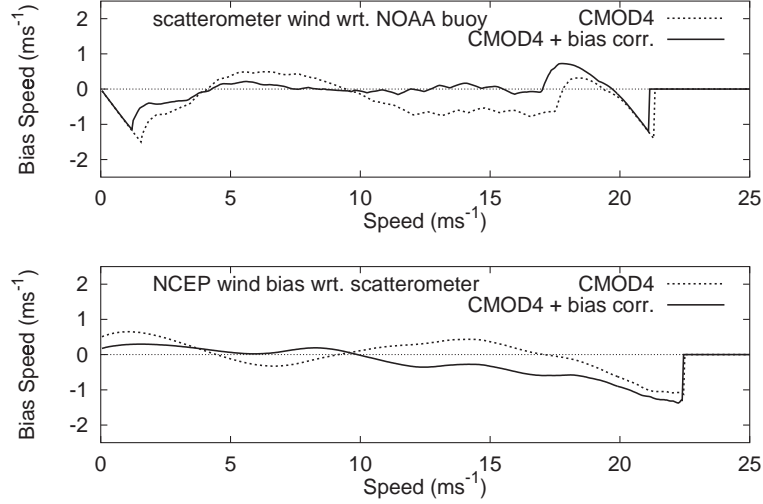


Figure 2: Higher order calibration by cumulative distribution mapping following [Stoffelen (1998)]. Top panel Shows the bias of the scatterometer wind with respect to the NOAA buoy. Bottom panel shows the bias of the NCEP wind with respect to the scatterometer. Wind speeds derived using CMOD4 are dotted lines in both panels. Solid lines have the above described additional bias correction.

speed transformation is given by:

$$\tilde{v} = \begin{cases} \bar{v} & \bar{v} \leq 15 \text{ms}^{-1} \\ 15 + a(\bar{v} - 15) + b(1 - a)(1 - \exp^{-(\bar{v}-15)/b}) & \bar{v} > 15 \text{ms}^{-1} \end{cases} \quad (11)$$

This type of function was chosen to obtain a smooth transition from the identity for wind speeds lower than 15ms^{-1} to a linear mapping different from the identity at higher wind speed. For high wind speeds the asymptotic behaviour is given by

$$\tilde{v} = (15 + b)(1 - a) + a\bar{v} \quad (12)$$

and the slope between \tilde{v} and \bar{v} is determined by a . Note that for $a = 1$ the transformation is the identity.

NRCS observations from Carswell show a dependence of the asymptotic slope of the wind speed transformation on incidence angle. This slope is fitted using a cubic function of θ as follows:

$$a(\theta) = -9.148 \cdot 10^{-1} + 4.438 \cdot 10^{-2}\theta - 5.093 \cdot 10^{-4}\theta^2 \quad (13)$$

Next the value of b is chosen such that for wind speeds of approximately 45m/s the backscatter σ_0 observed by Donnelly and Carswell corresponds to the

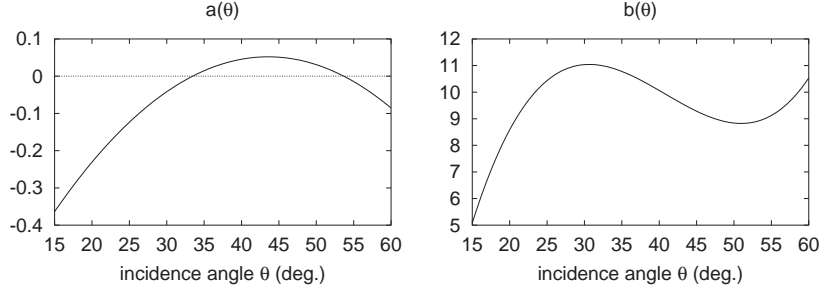


Figure 3: Graph of the two functions $a(\theta)$ and $b(\theta)$.

backscatter measured by CMOD4 by the wind speed $\tilde{v}(45)$. The value b lies for incidence angles between 18 and 60 degrees in the range from 9 to 11,

$$b(\theta) = -1.928 \cdot 10^1 + 2.475\theta - 6.469 \cdot 10^{-2}\theta^2 + 5.286 \cdot 10^{-4}\theta^3 \quad (14)$$

The transformation of the wind speed is only applied to the definition of B_0 in CMOD4. The first and second harmonic B_1 and B_2 are changed only by the low and medium wind speed bias correction. Figure 3 shows a graph of the two function $a(\theta)$ and $b(\theta)$. Note that $a(\theta)$ is only positive for incidence values between approximately 33 and 53 degrees. Incidence values outside this range have a negative slope which implies that two different wind speed values correspond to the same B_0 . This saturation behaviour was already observed by ([Carswell (1999)]).

Although the wind speed domain mapping did not change the first harmonic, the current used description of B_1 is not correct. For high wind speeds observations ([Donnelly (1999)] and [Carswell (1999)]) show that the first harmonic decreases to values near zero. A scaling factor is introduced to obtain this asymptotic behaviour and is shown in Fig. 4. This scaling factor is defined as

$$f(x) = \begin{cases} 1 & x < 15 \\ \exp(-(x - 15)^2 \cdot 6.4 \cdot 10^{-3}) & x \geq 15 \end{cases} \quad (15)$$

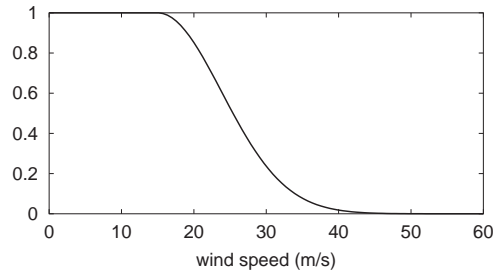


Figure 4: Scaling factor of B_1

As in the previous section, determining the bias of the previously mentioned data set of triple collocated scatterometer, NOAA buoy and NCEP wind observations the influence of both corrections (low and medium wind bias and the high wind correction) is shown in Fig. 5 together with only low and medium wind speed correction applied to CMOD4. By construction the low wind speed biases do not

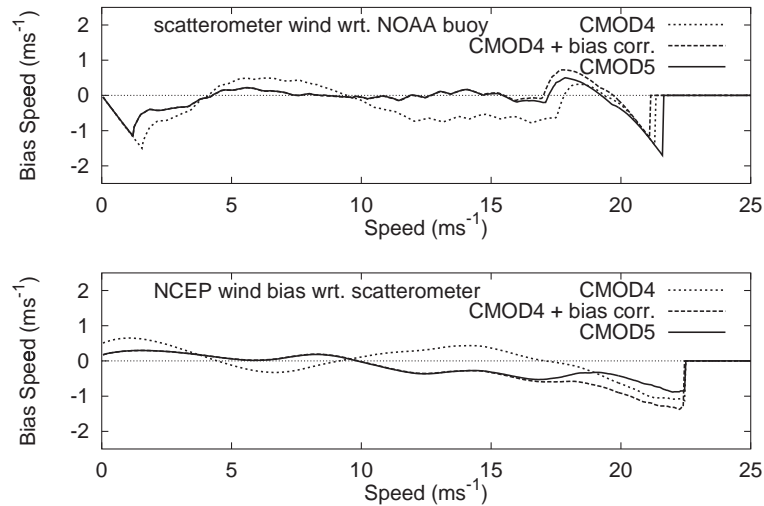


Figure 5: Higher order calibration by cumulative distribution mapping following [Stoffelen (1998)]. Top panel Shows the bias of the scatterometer wind with respect to the NOAA buoy. Bottom panel shows the bias of the NCEP wind with respect to the scatterometer. Wind speeds derived using CMOD4 are dotted lines in both panels, dashed lines have the above described additional bias correction and the dashed lines is the bias derived using CMOD4 low and medium wind speed bias correction and high wind speed correction (called CMOD5).

change by the addition high wind speed correction. Wind speeds larger than 17 ms^{-1} from CMOD5 have smaller biases than CMOD4 and CMOD4 with low and medium wind speed corrections. Only NOAA buoy wind speeds of approximately 22 ms^{-1} have a little worse bias; this is due to the small number of observations used to determine the bias between scatterometer and NOAA buoy wind speed.

4 CMOD5 performance

In this section the new GMF as constructed in the previous section is compared to the GMF as presented by Donnely and Carswell and is applied onto a data set of high wind observations compared to 10 meter wind from the European Centre for

Middle Range Forecast (ECMWF). From now on this new GMF is called CMOD5. First a comparison is made with data and the CMOD4HW GMF as described by Donnelly et al. [Donnelly (1999)]. Their work showed NRCS observations in a wind speed range between 5 and 45 ms^{-1} . Next, the GMF as constructed by Carswell is compared to CMOD5 in a wind speed range between 25 up to 60 ms^{-1} . The last part of this section is dedicated to comparison with ECMWF 10 meter wind.

4.1 CMOD5 compared to other GMFs

In Fig. 6 the CMOD5 GMF is shown together with CMOD4HW as described in [Donnelly (1999)] for four incidence angles. Backscatter measurements were collected over a 2-year period during five separate field experiments with an air-

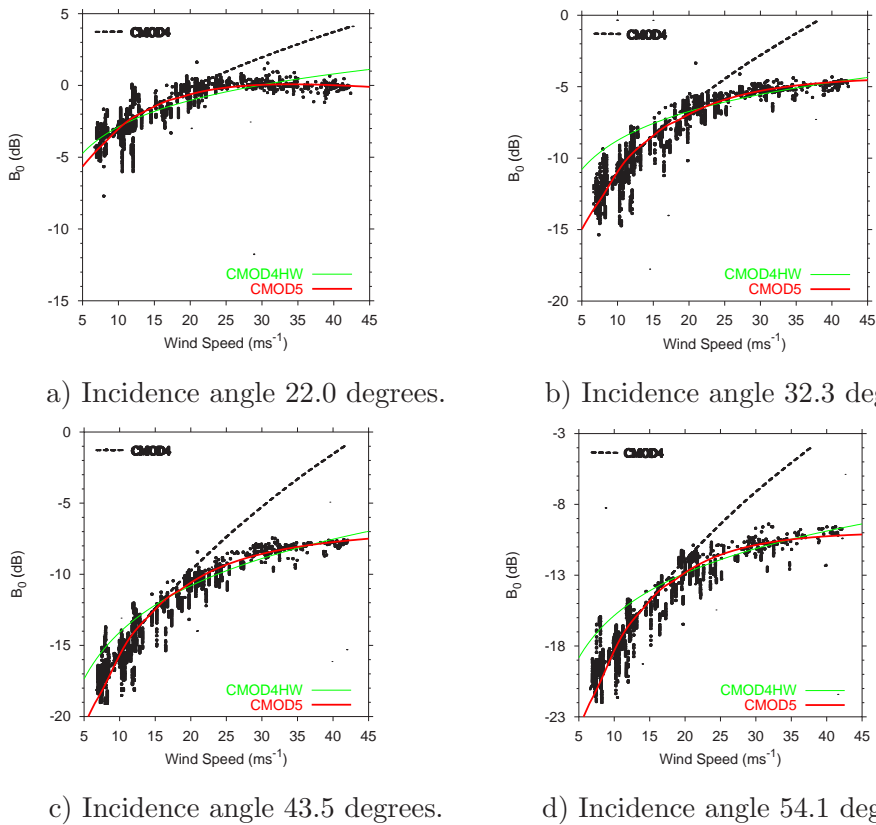


Figure 6: Mean NRCS B_0 for GMF's CMOD4 ([Stoffelen (1997b)]), CMOD4HW ([Donnelly (1999)]) and the new CMOD5 GMF. Mean NRCS backscatter measurements as presented by [Donnelly (1999)].

borne scatterometer. Most of the wind estimates above 20 m s^{-1} were derived from flight level data or GPS dropsonde data. The flight level derived winds are based on a boundary layer model. The GPS dropsonde raw wind estimates is believed to be equivalent to 10-30 second averaged buoy winds.

The data points in Fig. 6 are either single dots or appear as a column of dots. Airborne backscatter observations may be less accurate than spaceborne observations due to small errors in position and orientation of the air plane. Each ERS satellite has a number of gyroscopes to 'steer' the spacecraft and therefore the errors in orientation are small. Furthermore, the wind derivation from either flight level or GPS dropsonde data may also introduce some errors. The column data points are probably the result of this. The single dots do not have this behaviour and are suspected to originate from a more stable experiment. CMOD4HW was obtained by fitting the mean of the NRCS observations in 2 m s^{-1} bins.

For the wind speed range shown in Fig 6, CMOD5 follows approximately the mean of the observed backscatter B_0 . Note the saturation behaviour at the lowest incidence angle (Fig. 6a).

In Fig. 7 the CMOD5 GMF is shown together with CMOD4HW as described in [Donnelly (1999)] and HighWind as described in [Carswell (1999)], for a wind speed range from 25 to 60 m s^{-1} and for the same four incidence angles as in Fig. 6. The discrepancy for wind speeds from 25 to approximately 35 m s^{-1} is due to the

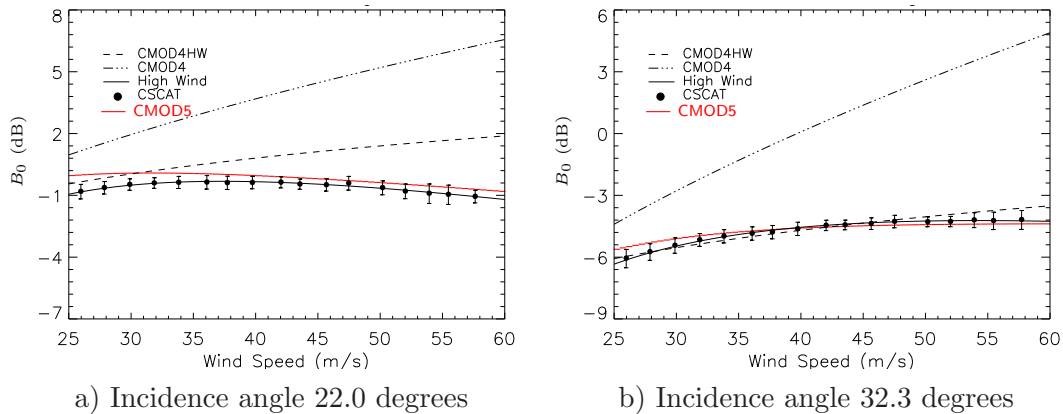
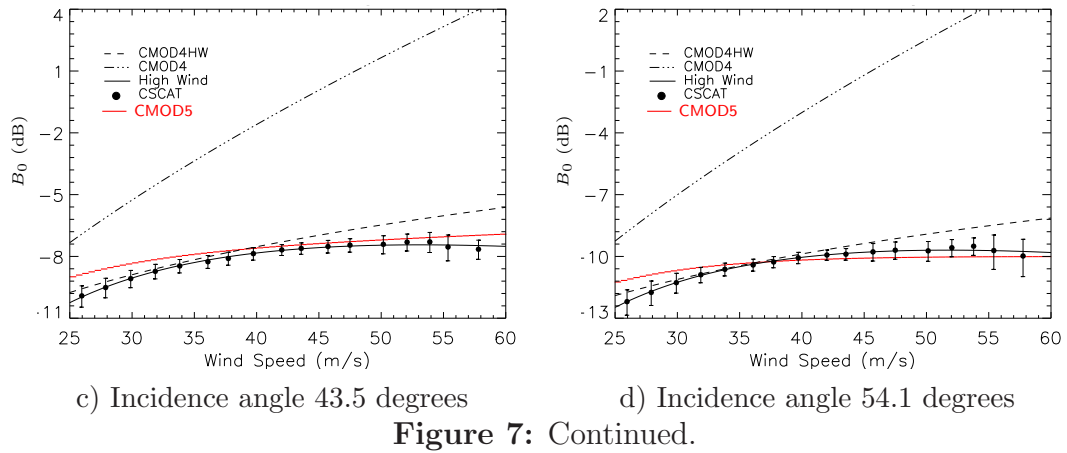


Figure 7: Average B_0 measurements (solid circles) from [Carswell (1999)] are plotted versus the mean 10 meter wind. Standard deviations of the B_0 measurements within 2 m s^{-1} wind speed bin are shown by vertical lines. NRCS B_0 from CMOD4 (dashed dotted line, [Stoffelen (1997b)]), CMOD4HW (dashed line, [Donnelly (1999)]) HighWind (solid black line [Carswell (1999)]) and CMOD5 (solid red line, section 3) GMFs.



fact that CMOD4 is used for low wind speeds and a smooth transition is created to higher wind speeds. Note the large difference between CMOD4 and the other GMFs.

The observations of the first harmonic B_1 as presented by [Carswell (1999)] is shown in Fig. 8 together with the GMF CMOD4, CMOD4HW, HighWind and CMOD5. Apart from CMOD4 all GMFs have a zero asymptotic behaviour. In Fig. 9 observations of the second harmonic are shown together with the GMFs. The GMF CMOD4 and CMOD5 have a little higher value for the second harmonic than the other GMFs and the measurements as presented by [Donnelly (1999)]. The difference is however not very large and the second harmonic of CMOD5 is therefor not adjusted.

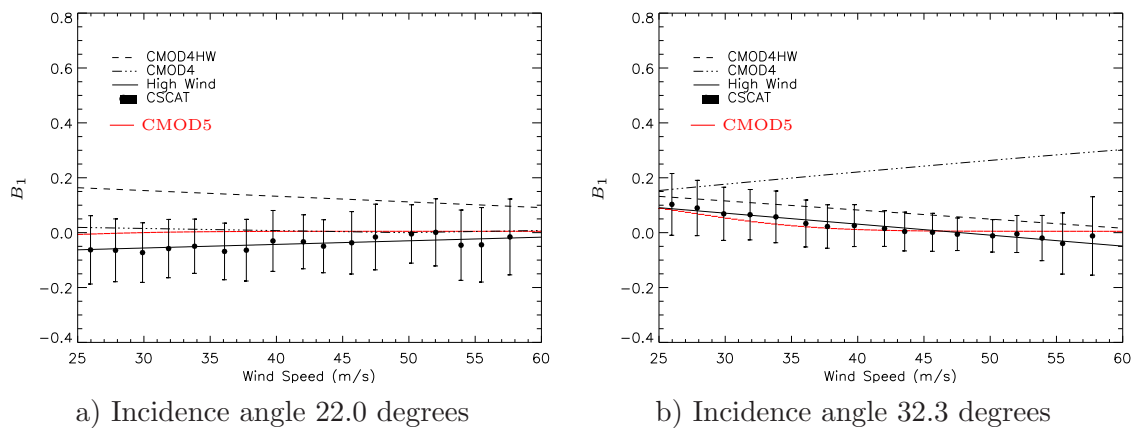


Figure 8: First harmonic B_1 versus mean 10 meter wind. See caption of Fig. 7 for explanation of lines and symbols.

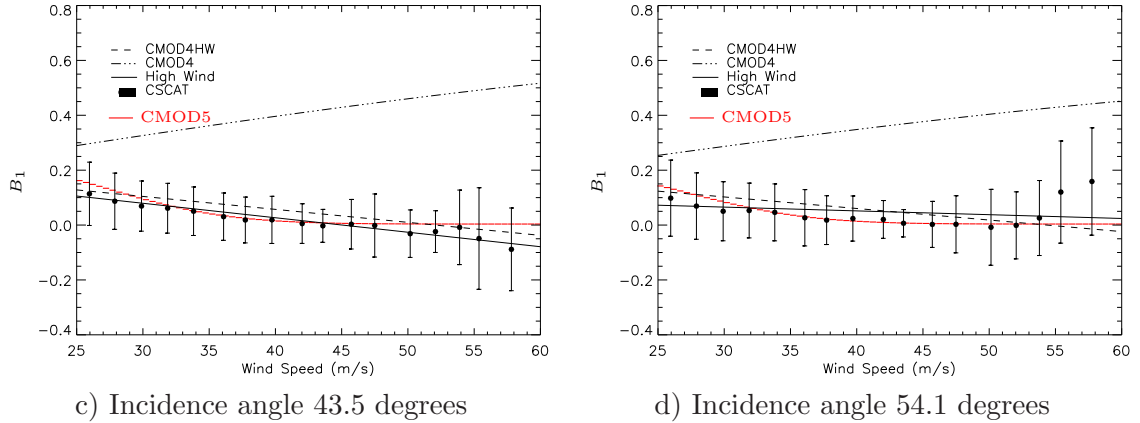


Figure 8: Continued.

4.2 Comparison with ECMWF 10 meter wind

Data from the ERS satellites are processed using CMOD4 and CMOD5. ERS observations are transmitted in messages containing 19×19 observations. In the period from August 1998 to December 1998 all messages with a CMOD4 wind speed larger than 18 m s^{-1} were collected. For each observation in this data set the first guess ECMWF was obtained by spatial interpolation of T213 ECMWF fields. Time interpolation is performed on three successive first guess fields from the 4DVAR suite to obtain collocated observations. The ERS messages are screened

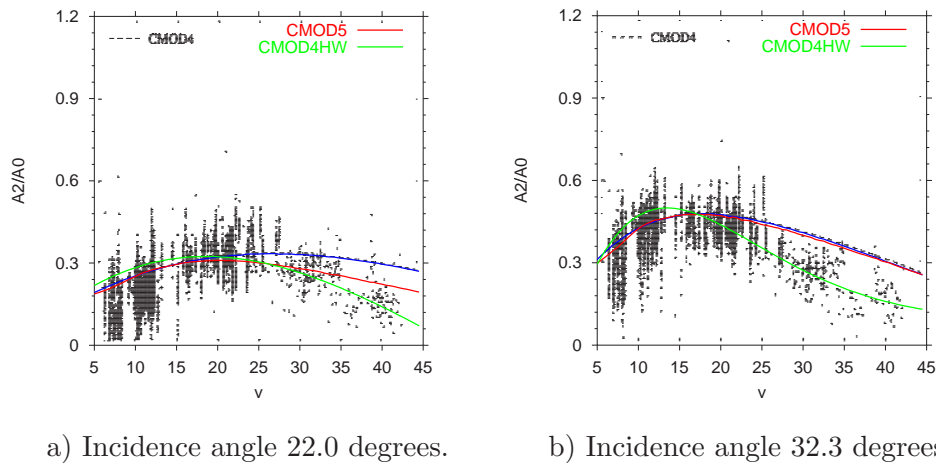
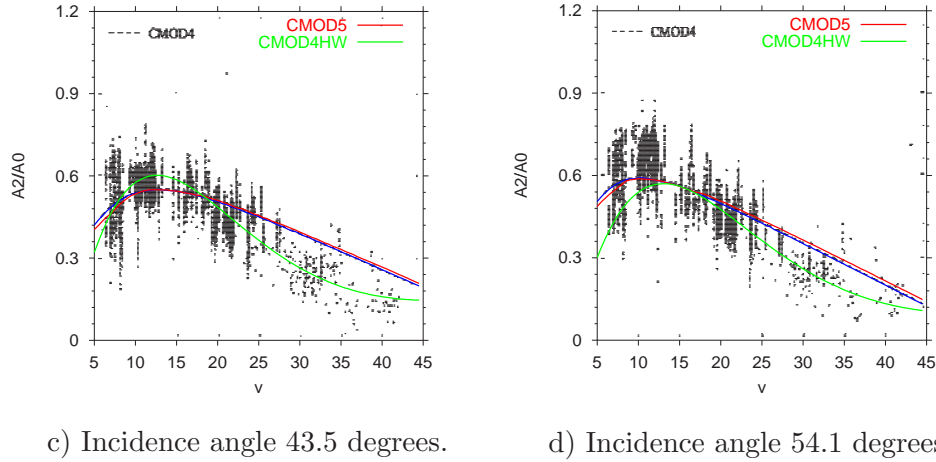


Figure 9: Second harmonic B_2 for GMF CMOD4 ([Stoffelen (1997b)]), CMOD4HW ([Donnelly (1999)]) and the new CMOD5 GMF.

**Figure 9:** Continued.

and the ambiguity problem is solved using PRESCAT, ([Stoffelen (1997a)]) for both CMOD4 and CMOD5. The resulting wind statistics are shown in Table 1. The

$N = 22076$	type	mean	RMS
Speed	CMOD4	14.0	14.6
	CMOD5	14.4	15.0
	ECMWF	14.7	15.3
Direction	CMOD4	38.4	104.3
	CMOD5	39.1	105.0
	ECMWF	44.1	103.5
u -compon.	CMOD4	-5.7	11.0
	CMOD5	-5.9	11.4
	ECMWF	-6.6	12.1
v -compon.	CMOD4	0.7	9.5
	CMOD5	0.7	9.8
	ECMWF	0.8	9.4

Table 1: Wind statistics for the selected ERS data set for CMOD4, CMOD5 and ECMWF.

number of observations used in these statistics is 22076. In general the mean values of the CMOD5 wind lie closer to the ECMWF wind than CMOD4. The RMS for CMOD5 are closer to ECMWF for wind speed and the u -component of the wind, while in for other types the RMS corresponding to CMOD4 is closer to

the ECMWF RMS.

In Table 2 the statistics for the differences between two of the three types is presented. The wind speed difference for the three differences reveal that the CMOD5 wind speed lies closer to the ECMWF wind speed. The correlation of the difference between CMOD5 and ECMWF is also higher than any of the other correlations. This implies that CMOD5 can be better explained by ECMWF data. No change in mean difference with respect to the direction between ECMWF and the GMFs CMOD4 and CMOD5 is observed.

$N = 22076$	type	mean	RMS ²	Corr.
Speed	CMOD4 - ECMWF	-0.631	5.713	220.804
	CMOD5 - ECMWF	-0.244	5.637	227.794
	CMOD4 - CMOD5	-0.387	0.645	218.701
Direction	CMOD4 - ECMWF	1.601	623.091	8910.787
	CMOD5 - ECMWF	1.651	392.568	9084.287
	CMOD4 - CMOD5	-1.419	272.372	10507.049

Table 2: Wind difference statistics for the selected ERS data set.

Fig. 10 shows the wind speed cumulative distribution mapping. In this figure the bias of the ECMWF wind speed with respect to the CMOD5 wind speed is denoted by a solid line. The bias of CMOD5 with respect to CMOD4 is designated by a dashed line and the bias of CMOD4 with respect to ECMWF is the dotted line. Clearly visible is the reduction of the bias in ECMWF 10 meter wind with

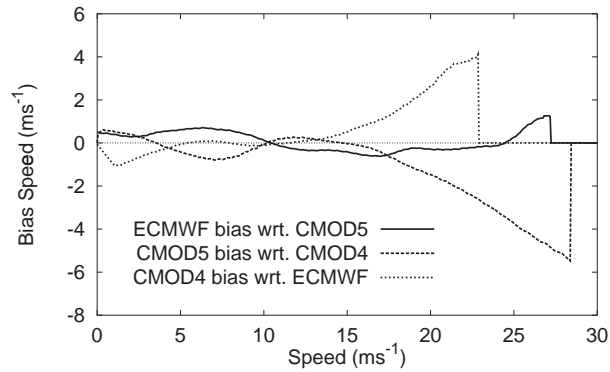


Figure 10: Higher order calibration by cumulative distribution mapping following [Stoffelen (1998)]. Shown here is the bias of the ECMWF wind speed with respect to the CMOD5 wind speed (solid line), bias of CMOD5 with respect to CMOD4 (dashed line) and the bias of CMOD4 with respect to ECMWF (dotted line).

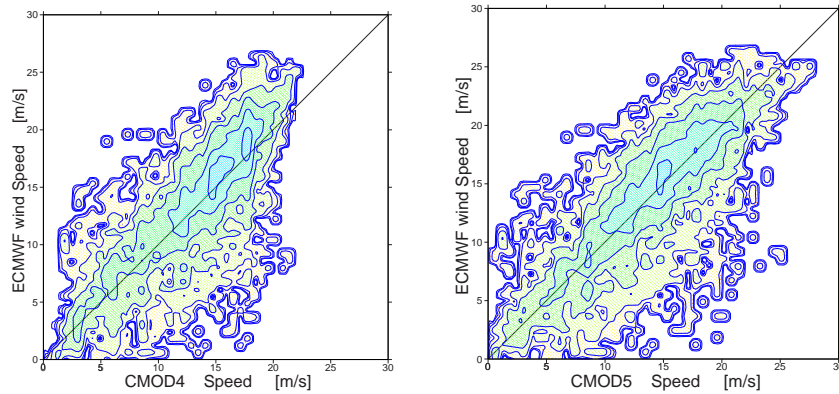


Figure 11: Scatter plot of ECMWF 10 meter wind versus CMOD4 and CMOD5 scatterometer wind.

respect to CMOD5 wind estimates. The increase of bias for CMOD5 wind speeds around 23 ms^{-1} is most likely due to the small number of observations for this wind speed in the data set. The graph of the bias of CMOD5 wind speed with respect to CMOD4 wind speed is related to the introduced wind speed mapping.

In Fig. 11 the scatter plots of ECMWF 10 meter wind speed versus CMOD4 wind speed and CMOD5 wind speed is shown. The CMOD5 scatterometer wind speed has a much better scatter plot with respect to ECMWF 10 meter wind than CMOD4 scatterometer wind.

In Fig. 12 the distribution of the maximum likelihood estimate (MLE) of both CMOD4 and CMOD5 is shown versus the wind speed. The MLE is the normalized distance to the wind cone; positive MLE corresponds to observations inside the wind cone, while negative values lie outside the wind cone.

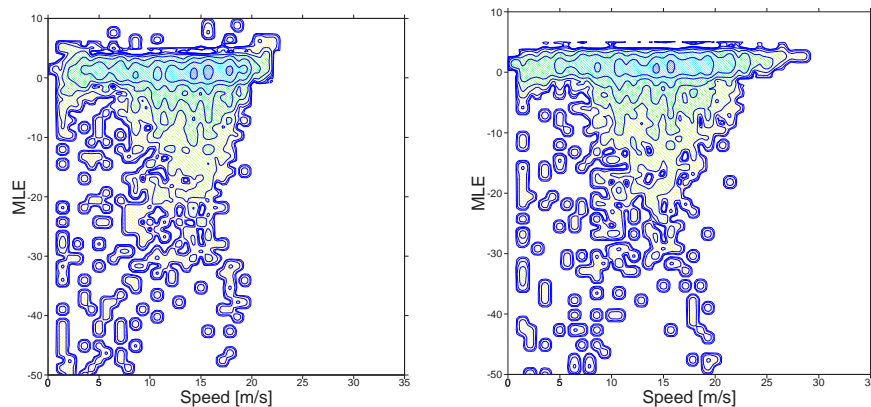


Figure 12: Scatter plot of the MLE versus scatterometer wind speed from CMOD4 and CMOD5 scatterometer wind.

The MLE as obtained using CMOD5 has a clear extreme value of around 5, while CMOD4 MLE has values larger than 5. For small wind speeds (smaller than 10 m s^{-1}) the number of backscatter observations using CMOD5 inside the wind cone is decreased with respect to the number of CMOD4. Wind speeds in the medium range of both GMFs have more or less the same MLE distributions. CMOD4 has a large amount of points inside the cone for wind speeds around 20 m s^{-1} (Fig. 12 left panel). For CMOD5 the majority of MLE for high wind speeds are small, implying close to the wind cone.

In the left panels of Fig. 13 the projections of backscatter triplets on the $\sigma_0^{\text{fore}} = \sigma_0^{\text{aft}}$ -plane are shown for nodes 3, 11 and 19. The corresponding wind speed is shown in the colour scale. The dots are the projected backscatter observations from the selected period. These dots are wind speed coloured according to the shown colour scale. The used wind speed originates from ECMWF.

In all three left panels in Fig. 13 we clearly see the saturation behaviour of CMOD5. The ECMWF wind speed is scattered with wind speeds ranging from 15

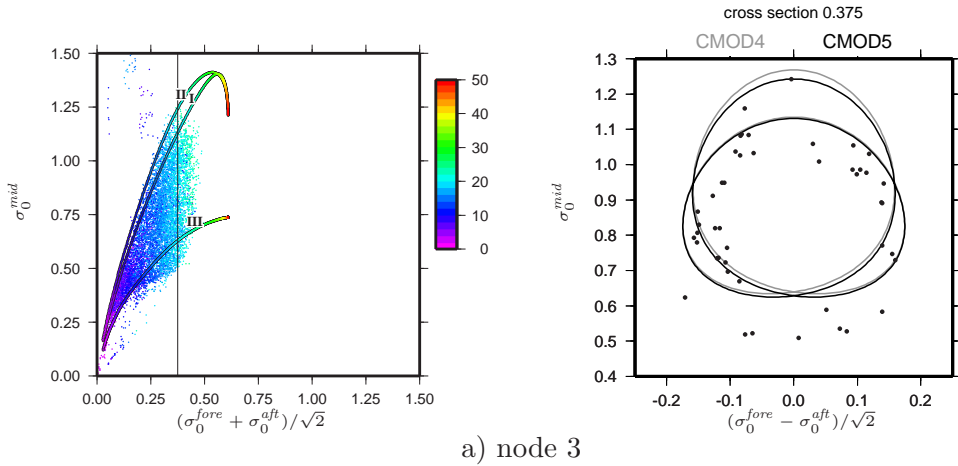


Figure 13: Left panels show cross section of CMOD5 with the $\sigma_0^{\text{fore}} = \sigma_0^{\text{aft}}$ -plane together with projected backscatter observations (ECMWF wind speed coloured). The three curves show CMOD5 at upwind (I), downwind (II) and crosswind (III). The right panels show intersections with a plane perpendicular to the plane in the left panel, positioned at the vertical line in the left panel. Intersection with CMOD4 is in grey; CMOD5 in black. Points are observations with a distance smaller than 0.001 to this plane.

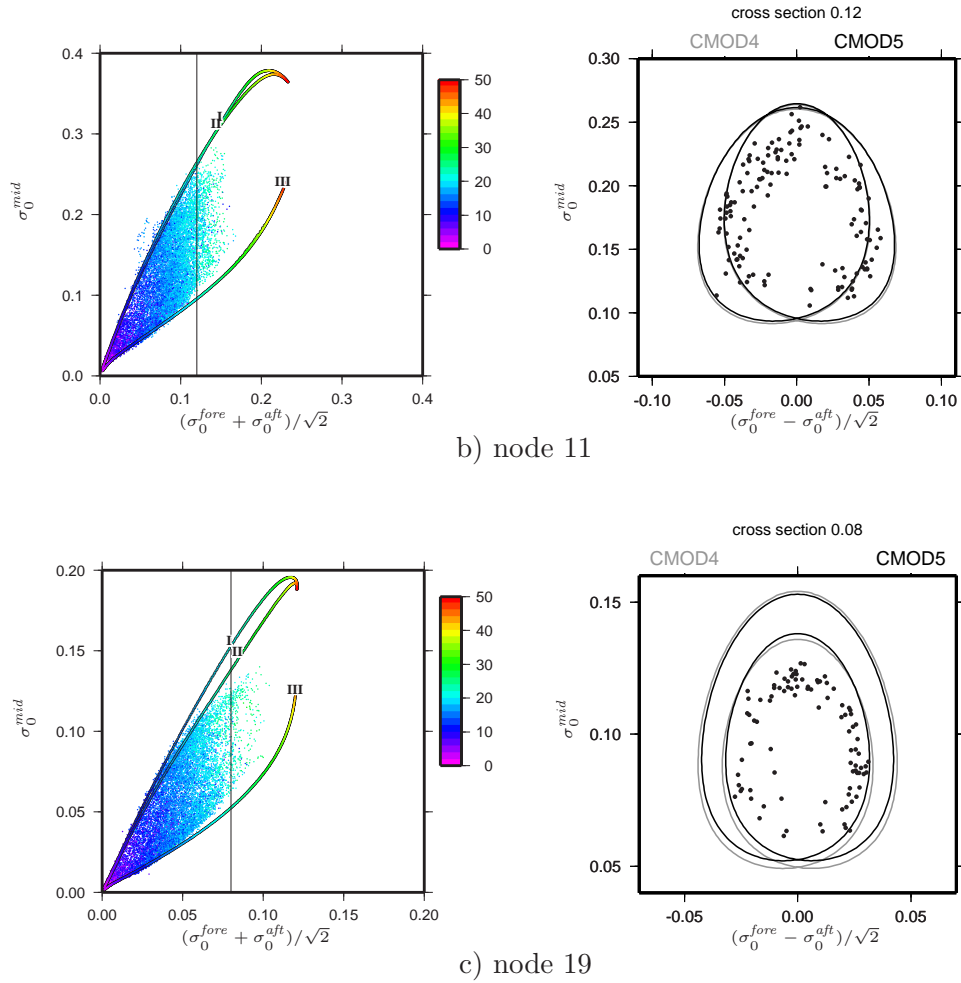


Figure 13: Continued.

ms^{-1} to around $20 ms^{-1}$. This scatter is also visible in the right panel of Fig. 11.

The right panels of Fig. 13 show the cross section perpendicular to the $\sigma_0^{fore} = \sigma_0^{aft}$ -plane at the position of the vertical line in the left panel. The black dots in this cross section are backscatter observations which have a distance of less than 0.001 to the plane. The black line is the intersection of CMOD5 with the plane under consideration; the grey line originates from CMOD4 and is plotted as a reference to the changed wind cone. Almost all backscatter observations lie inside the cone, corresponding to a negative MLE. Furthermore, CMOD5 fits the projected data

very well for node 11 and 19 for wind speeds smaller than 15 m s^{-1} (i.e. small backscatter values) as can be seen from Fig. 13(b) and (c) left panels. For node 3 however, there are a number of observations clearly outside the wind cone, see Fig. 13 left and right panel.

4.3 High wind cases

To show the consistence between scatterometer winds and ECMWF model, four cases were selected from high wind observations used in the previous section. The cases cover a tropical cyclone in the Atlantic, a low pressure system in the North Pacific, Trade winds in the South Atlantic and a low pressure system near Island.

In Fig. 14 the wind pattern off the tropical cyclone Danielle is shown as observed by ERS at 31 August 1998 at 0329 UTC north of the Bahama Islands. The left panel shows the ECMWF wind field, the middle panel contains wind arrows as observed by ERS using the CMOD4 GMF and the right panel shows the corresponding CMOD5 GMF wind field. Black arrows are wind speeds smaller than 10 m s^{-1} . The ECMWF wind is underestimated in the neighborhood of the cyclone, where both ERS observed wind speeds are larger than 10 m s^{-1} . In the center of the cyclone wind speeds a little above 30 m s^{-1} were observed by CMOD5. The ambiguity removal scheme as implemented in PRESCAT, [Stoffelen (1997a)] shows some incorrect solutions for both GMFs. This is due to the fact the ECMWF wind field is used to select one of the two scatterometer wind solutions and the

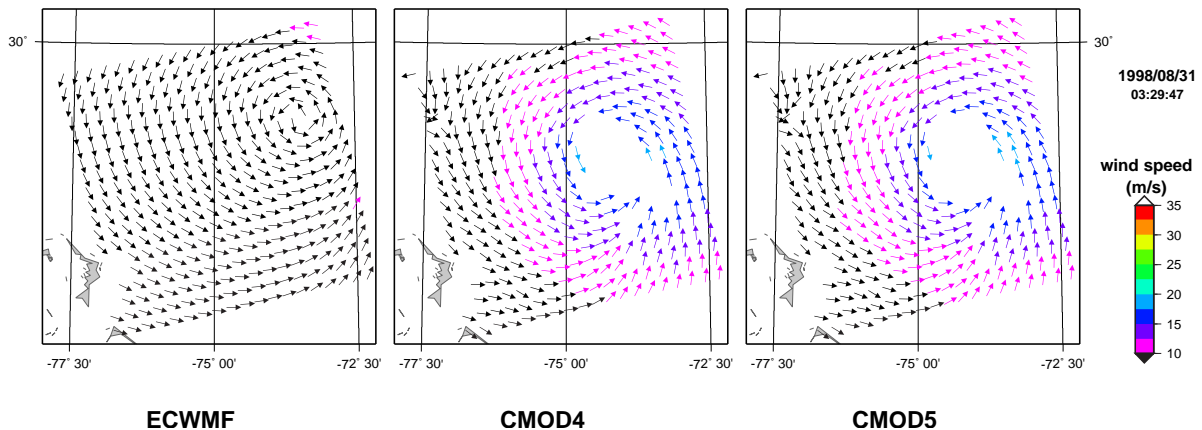


Figure 14: Tropical cyclone Danielle on 31 August 1998 at 0329 UTC just above the Bahama Islands. In the left panel the ECMWF wind field is shown. The middle panels shows the scatterometer wind as observed by ERS using CMOD4; the right panel shows ERS with CMOD5. Arrows with wind speeds lower than 10 m s^{-1} are colored black.

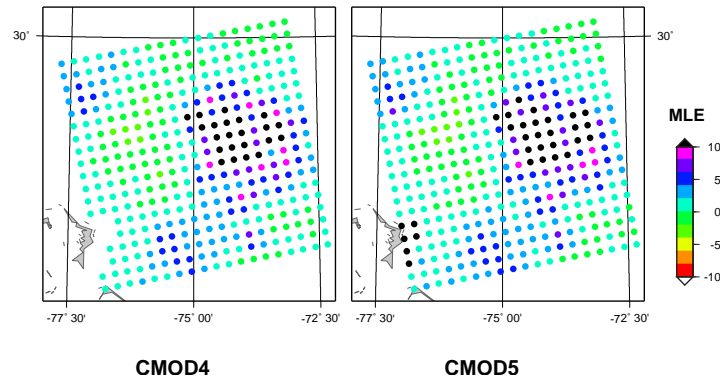


Figure 15: Maximum likelihood estimate of CMOD4 and CMOD5 for the cyclone Danielle as shown in Fig. 14.

ECMWF wind field miss-positioned this cyclone. Quality control of PRESCAT is used to omit erroneous winds. This results on the white region in the center of the cyclone. Note also that at the west boundary of the eye of the cyclone there is one ERS wind observation less for CMOD5 compared to CMOD4. In Fig. 15 maximum likelihood estimate (MLE) of both CMOD4 and CMOD5 is shown. The MLE is the normalized distance to the wind cone. Figure 15 shows a reduction in MLE at the position of the cyclone for CMOD5 with respect to CMOD4. In both panels the influence of the cyclone on the MLE is clearly visible as an increase in MLE (blue to purple colored dots).

In Fig. 16 the wind fields of ECMWF and the scatterometer wind from CMOD4 and CMOD5 are shown for a case in the North Pacific on 10 November 1998 at 0943 UTC. A low pressure system is positioned around 42°N and 165°W . ECMWF wind speeds close to this system have values just over 25 m s^{-1} . CMOD4 wind speeds are clearly smaller, just over 20 m s^{-1} , while CMOD5 wind speeds higher: just below 30 m s^{-1} . The quality control in PRESCAT is not changed when using CMOD5. This results in a different quality check as can be seen in Fig. 16 by the different number of displayed arrows for CMOD4 and CMOD5. The inversion routine from PRESCAT to estimate the wind speed and direction from a backscatter triplet is changed slightly. The first guess wind speed used by the inversion is chosen to be equal to the previously determined wind speed. This causes problems for the next inversion when the inversion did not find a valid wind speed. To overcome this problem a maximum wind speed of 20 m s^{-1} is set to the first guess wind speed. An improved inversion scheme is required to obtain more reliable results from the inversion.

In Fig. 17 the normalized distance to the wind cone of CMOD4 and CMOD5 is shown. The values are smaller for CMOD5 than for CMOD4. Note also that the wind speed ambiguities have small MLE values.

ERS observation together with ECMWF wind fields in the South Atlantic ocean on 17 November 1998 at 0354 UTC is shown in Fig. 18. The ECMWF winds show an increase in wind speed in the middle of the swath; CMOD5 high wind speeds in the middle of the swath. The top part of the swath shown in Fig. 18 has scatterometer observations with wind speeds smaller than ECMWF wind speeds. The direction of all three wind observations have a striking resemblance in this part of the swath. Below 55°S a small front appears in the both scatterometer observations, while the ECMWF wind direction remains almost unchanged. Scatterometer wind observations to the west of this front have a smaller wind speed than the ECMWF wind. Note that in the bottom left corner of the swath the ambiguity removal scheme applied here is results in awkward wind directions for both CMOD4 and CMOD5. In Fig. 19 the MLE of both GMFs are shown. Again CMOD5 has generally lower MLE's.

The last case shown here is a low pressure system close to Island at 27 November 1998, ERS observation from 1252 UTC. Clearly The CMOD5 wind speed has more resemblance with ECMWF than CMOD4. The position of the ECMWF low pressure system lies a little bit to the south west with respect to the position as

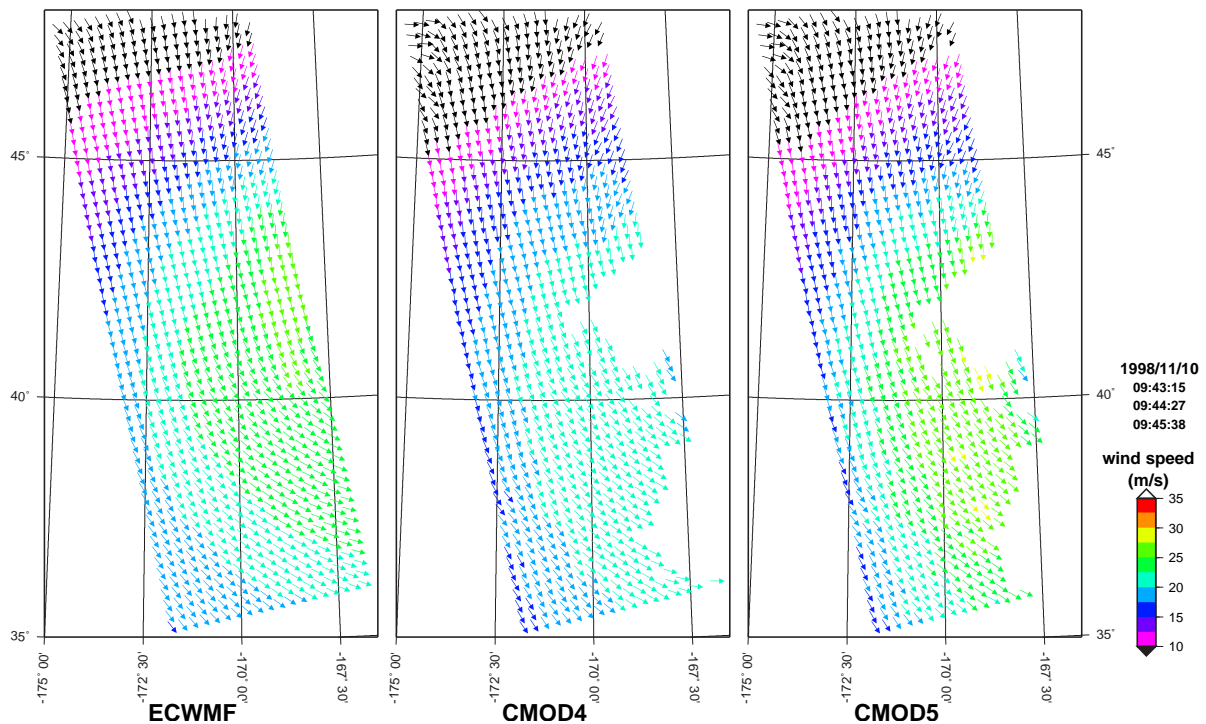


Figure 16: Wind fields in the North Pacific (175°W and 42°N) from ECMWF, CMOD4 and CMOD5.

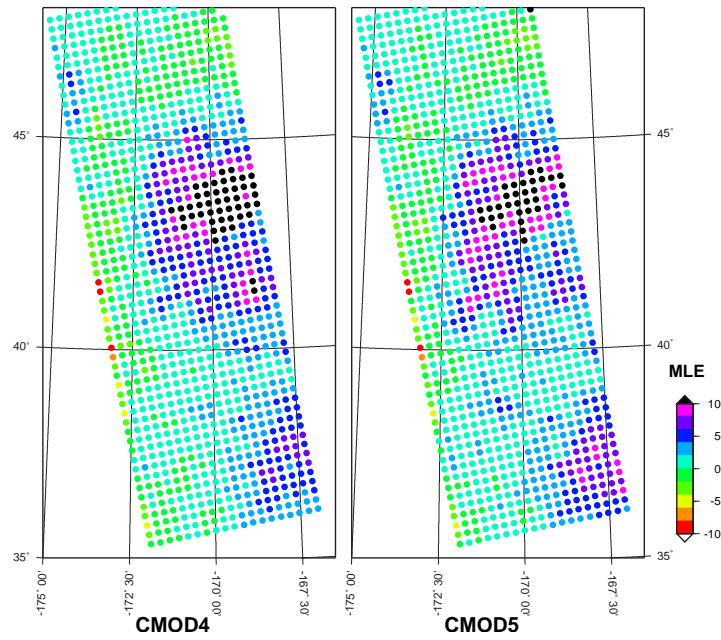


Figure 17: Maximum likelihood estimates as observed by CMOD4 and CMOD5 for the scatterometer winds shown in Fig. 16.

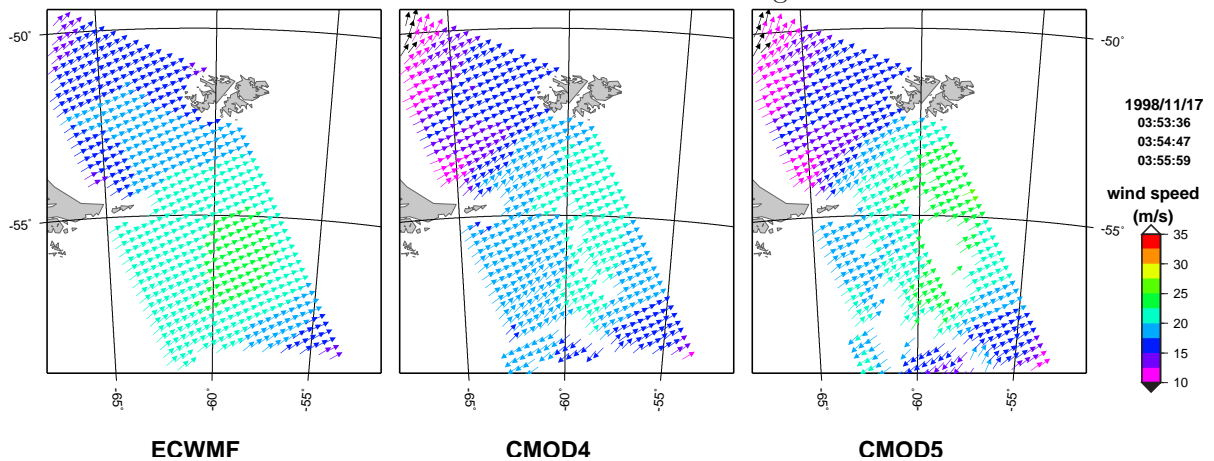


Figure 18: Wind fields in the South Atlantic (60°W and 55°S) from ECMWF, CMOD4 and CMOD5. Wind speeds smaller than 10 m s^{-1} are colored black.

observed by ERS. The MLE from CMOD5 shown in Fig. 21 shows some signal of the low pressure region (blue, purple and black dots).

5 Conclusions

In this text an improvement of the geophysical model function (GMF) CMOD4 is constructed. The improvement is primarily based on a mapping of the windspeed domain. Additional to the wind speed mapping the harmonic coefficients at high wind speeds are brought in line with those obtained by [Carswell (1999)] in aircraft campaigns.

The new GMF showed to have better agreement with ECMWF wind speeds for a number of high wind cases. A further improvement to fit the wind cone in the σ_0 -space of ERS is being performed at ECMWF.

References

- [Donnelly (1999)] Donnelly, W.J., J.R. Carswell, R.E. McIntosh, P.S. Chang, J. Wilkerson, F. Marks and P.G. Black, Revised Ocean Backscatter Models at C and Ku-band under High-wind Conditions, *J. Geophys. Res.*, **104** (C5) p 11485-11497, 1999
- [Carswell (1999)] Carswell, J.R. , A. Castells and E.J. Knapp, P.S. Chang, P.G. Black and F. Marks, Observed Saturation in C and Ku-band Ocean Backscatter at Hurricane Force Winds, *J. Geophys. Res.*, **104** (C5) p 11485-11497, 1999
- [Stoffelen (1997a)] Stoffelen, A.C.M, and D.L.T. Anderson, Ambiguity Removal and Assimilation of Scatterometer Data, *Q.J. Roy Meteorol. Soc.* **123**, p 491-518, 1997a

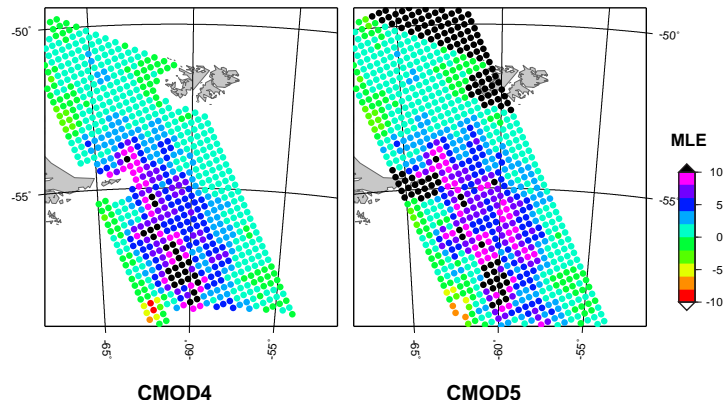


Figure 19: Maximum likelihood estimates as observed by CMOD4 and CMOD5 for the scatterometer winds shown in Fig. 18.

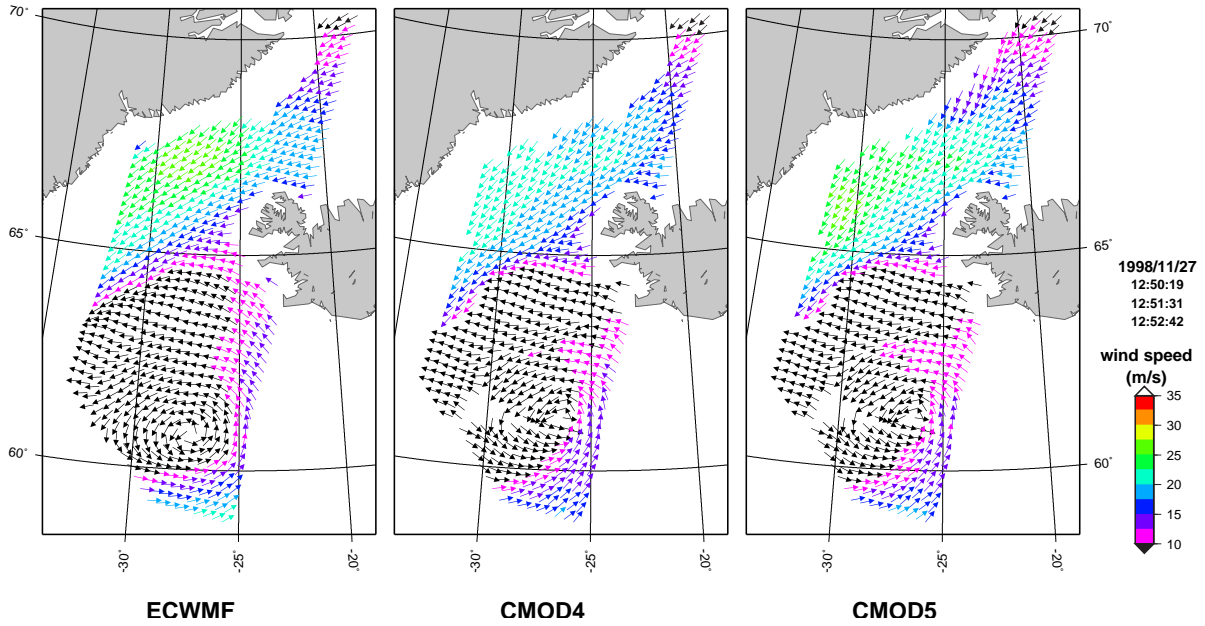


Figure 20: Wind fields in the North Atlantic (22°W and 65°N) from ECMWF, CMOD4 and CMOD5. Wind speeds smaller than 10 $m s^{-1}$ are colored black.

[Stoffelen (1997b)] Stoffelen, A.C.M, and D.L.T. Anderson, Scatterometer Data Interpretation: Derivation of the Transfer Function CMOD4, *J. Geophys. Res.*, **102** (C3) 5767-5780, 1997b

[Stoffelen (1998)] Stoffelen, A.C.M., Error Modeling and calibration; towards the true surface wind speed, *J. Geophys. Res.*, **103** (C4) 7755-7766, 1998

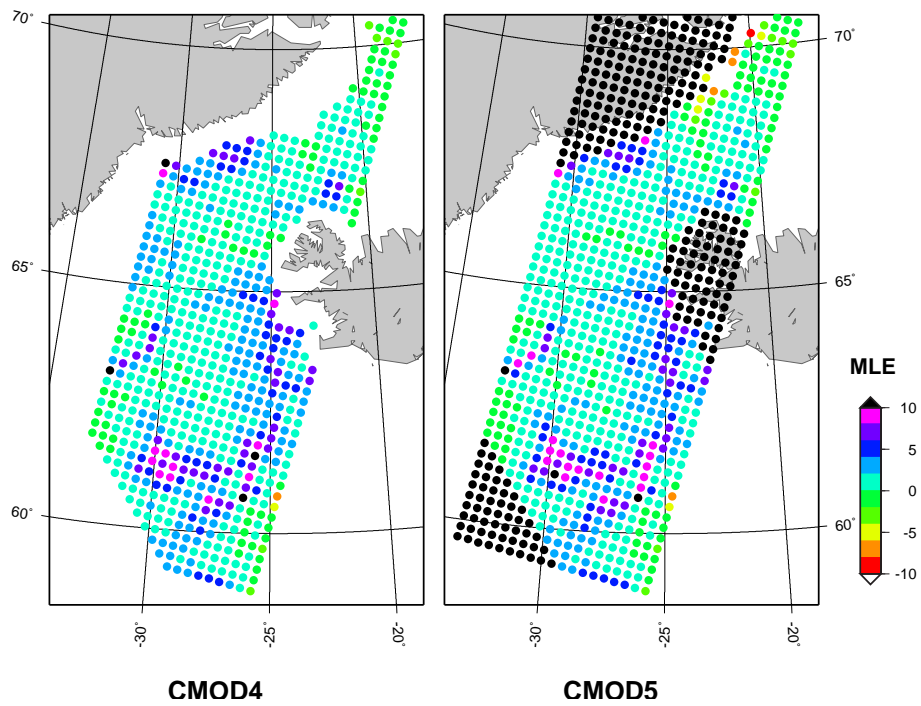


Figure 21: Maximum likelihood estimates as observed by CMOD4 and CMOD5 for the scatterometer winds shown in Fig. 20.